Available online at www.sciencedirect.com
ScienceDirect
Trans. Nonferrous Met. Soc. China 25(2015) 3953−3958
Transactions of Nonferrous Metals Society of China
www.tnmsc.cn

Microstructure evolution of alumina dispersion strengthened copper alloy deformed under different conditions

Ling LI[1], Zhou LI[1,2], Qian LEI[2], Zhu XIAO[3], Bin LIU[1], Na LIU[1]

1. School of Materials Science and Engineering, Central South University, Changsha 410083, China;
2. State Key Laboratory of Powder Metallurgy, Changsha 410083, China;
3. Key Laboratory of Nonferrous Metal Materials Science and Engineering, Ministry of Education, Central South University, Changsha 410083, China

Received 26 November 2014; accepted 5 May 2015

Abstract: Microstructure and texture evolution of Cu−0.23%Al_2O_3 dispersion strengthened copper alloy, deformed at room temperature or cryogenic temperature, were investigated. The main textures in hot-extruded specimen were Brass {011} ⟨211⟩ and Cube {100} ⟨100⟩. Textures of Brass {011} ⟨211⟩ and Goss {011} ⟨100⟩ were observed in specimen after deformation at room temperature; while textures of Brass {011} ⟨211⟩, Goss {011} ⟨100⟩ and S {123} ⟨634⟩ were detected after deformation at cryogenic temperature. It is believed that the additional Al_2O_3 nanoparticles can result in dislocation pinning effect, which can further lead to the suppression of dislocations cross-slip. While in the specimen deformed at cryogenic temperature, both pinning effect and cryogenic temperature are responsible for the formation of Brass, Goss and S textures.

Key words: cryogenic deformation; microstructure; texture; dispersion strengthened copper alloy

1 Introduction

Copper alloys have been widely applied in electro-technique, electronic information technique, automotive industry, due to their superior electrical and thermal conductivities as well as excellent ductility and machinability [1,2]. Oxide dispersion strengthened copper alloys, such as Cu−Al_2O_3, Cu−TiB_2, Cu−ThO_2, Cu−Y_2O_3 and Cu−CaO [3,4], are newly innovated copper alloys, which boast high strength and electrical conductivity. In recent years, Cu−Al_2O_3 alloys have attracted a great deal of interest [5,6]. Most previous researches have been concentrated on the deformation behavior of Cu−Al_2O_3 alloys during deformation at room temperature. According to the results of their researches, Al_2O_3 nanoparticles show great influence on the deformation characteristics of Cu−Al_2O_3 dispersion strengthened copper alloy [7,8]. On one hand, Al_2O_3 nanoparticles act as dislocation source, and a large amount of dislocations multiply during deformation. On the other hand, the pinning effect of Al_2O_3 nanoparticles on long range motion of dislocations inhibits the creation of dislocation cells in Cu−Al_2O_3 dispersion strengthened copper alloys.

The advantages of cryogenic deformation are readily discernible, such as grain refinement, which enhances both the strength and hardness [9]; its inducement of deformation twinning or/and shear zone, which improves the strength without sacrificing conductivity [10]; and its promotion on the formation of deformation textures, which adjusts the anisotropic properties [11,12]. However, the microstructure evolution of Cu−Al_2O_3 dispersion strengthened copper alloys during cryogenic deformation has not yet been reported. This work focuses on the microstructure evolution of Cu−0.23%$A1_2O_3$ (volume fraction) alloy deformed at cryogenic temperature or room temperature, in order to fulfill the realization of optimum comprehensive properties.

2 Experimental

A Cu−0.23%$A1_2O_3$ alloy was produced using an

Foundation item: Project (51271203) supported by the National Natural Science Foundation of China; Project (YSZN2013CLD6) supported by the Nonferrous Metals Science Foundation of HNG-CSU, China; Project supported by the Program Between the CSC (China Scholarship Council) and the DAAD (German Academic Exchange Service)

Corresponding author: Zhou LI; Tel: +86-731-88830264; E-mail: lizhou6931@csu.edu.cn

DOI: 10.1016/S1003-6326(15)64044-4

internal oxidation process [13]. The process included: 1) induction melting of Cu−0.05%Al (mass fraction) alloy in mid-frequency induction furnace, 2) nitrogen atomization, 3) mixing of the atomized Cu−Al alloy with an oxidant, 4) oxidation at 1000 °C for 1 h, 5) hydrogen reduction at 900 °C for 1 h under a pressure of 27 MPa and a vacuum of 1.33×10^{-2} MPa, and 6) hot extrusion at 930 °C with a ratio of 20:1 to form the final cylinder with a diameter of 53 mm. Samples with dimensions of 30 mm (length) × 30 mm (width) × 20 mm (height) were cut from the hot-extruded rod. Multiple forging processes were carried out until the heights of samples were reduced from 20 to 4 mm (reduced by 80% in height) during deformation at both room and cryogenic temperatures. Specimens had been given cryogenic treatment in a liquid−nitrogen solution (−196 °C) for 30 min before each cryogenic temperature forging process.

Specimens for optical microscope observation were ground, polished and finally etched by a solution containing ferric chloride (5 g), hydrochloric acid (25 mL) and alcohol (100 mL). The microstructure of metallographic specimens was observed using a Leica optical microscope. Electron back-scattered diffraction (EBSD) analysis was carried on a Siron 200 scanning electron microscope equipped with EBSD detector, with a scanning area of 10 μm×10 μm and a scanning step size of 45 nm. The X-ray diffraction texture analysis was conducted on a D8 Discover X-ray diffractometer. The orientation distribution function (ODF) maps were calculated using the harmonic series expansion method (series rank 22, Gaussian smoothing 5°, orthorhombic sample symmetry). Fractions of texture components were calculated using a texture calculation software [14]. Specimens for EBSD and XRD texture analysis were surface treated by electro-polishing. Transmission electron microscopy (TEM) observation was performed using a JEOL−2100F transmission electron microscope. Specimens for TEM observation were reduced by jet-polishing in a solution containing 25% nitric acid and 75% methanol. The central sections of the samples were selected to observe the microstructure and texture evolution.

3 Results and discussion

3.1 Microstructure of materials

Figure 1 shows the metallographic microstructure evolution of Cu−Al_2O_3 alloy during deformation process. Equiaxed grains appeared in the hot-extruded specimens, with an average size of 50 μm, before deformation (Fig. 1(a)). Fiber-shape morphology occurred in the specimen after forging deformation at cryogenic temperature (CT) and room temperature (RT) with a reduction of 80% (Figs. 1(b) and (c)). Compared with the non-forging specimen, the grain boundaries of specimens forged at CT and RT became discontinuous, which suggested that initial grains were refined during forging deformation process. Furthermore, the average width of fibers in specimens forged at CT was less than that of specimens forged at RT.

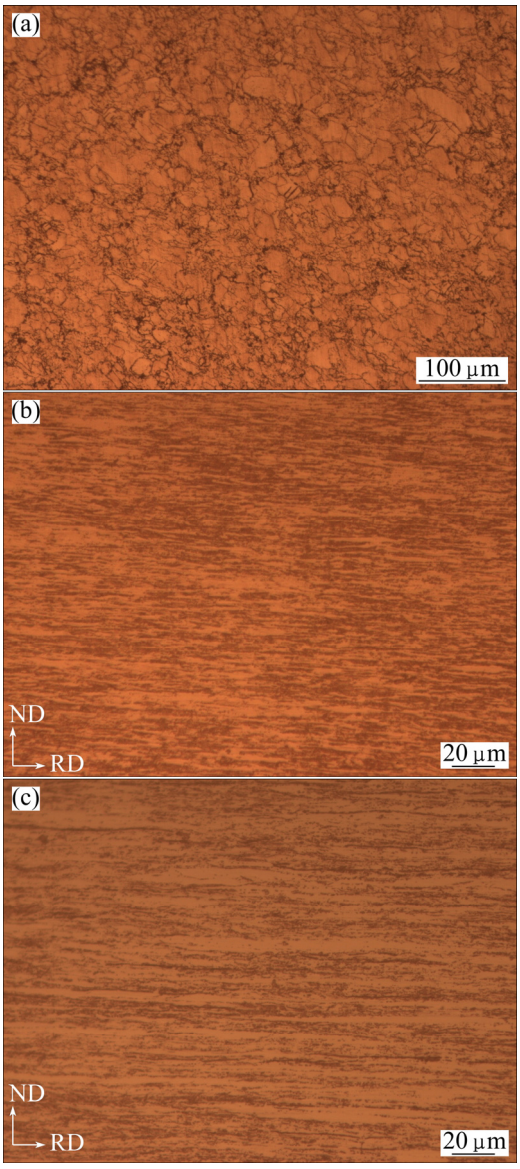

Fig. 1 Optical micrographs of hot-extruded Cu−0.23%Al_2O_3 alloy (a) and specimens forged at different temperatures with a reduction of 80%: (b) Cryogenic temperature; (c) Room temperature

Figure 2 shows the EBSD maps of the specimens after forging at CT and RT. Grains were compressed in transverse direction (TD), and many sub-boundaries were observed after forging deformation. Compared with grains deformed at RT (Fig. 2(b)), the sizes of grains deformed at CT were smaller (Fig. 2(a)). As shown in Fig. 3, the percentage of grains with the diameter less than 0.2 μm in specimens forged at CT was 87%

(Fig. 3(a)), while that in specimens forged at RT were 72% (Fig. 3(b)). Furthermore, a lager fraction of sub-grains (grains with misorientation angle less than 10°) formed in specimens forged at CT (Fig. 4(a)), compared with specimens forged at RT (Fig. 4(b)). Grains had been refined after cryogenic deformation.

As shown in Fig. 5, dislocations and dislocation cells appeared in specimens forged at CT (Fig. 5(a)) and RT (Fig. 5(b)). Besides, some layer structures with cross size of per flake less than 100 nm were observed in specimens forged at CT. Figure 5(a) shows the typical images of the flake in Cu−Al_2O_3 alloy forged at CT.

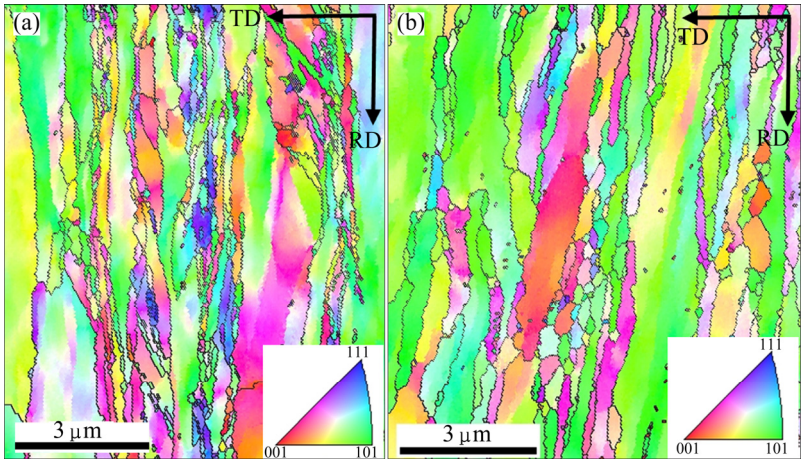

Fig. 2 EBSD inverse pole figure maps (longitudinal plane) of Cu−0.23%Al_2O_3 alloy deformed at different temperatures (For simplicity, only HABs are shown in maps): (a) Cryogenic temperature; (b) Room temperature

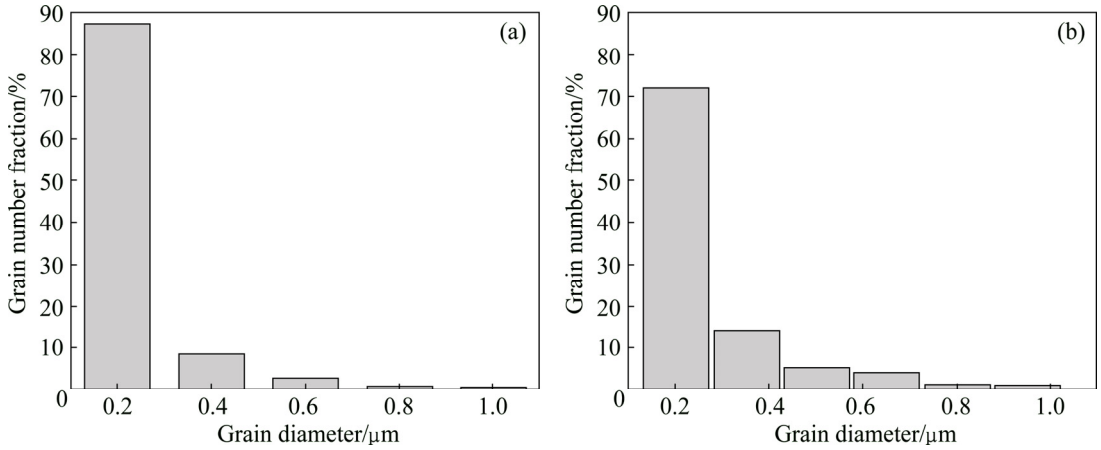

Fig. 3 Grain size distributions of Cu−0.23%Al_2O_3 alloy forged at different temperatures: (a) Cryogenic temperature; (b) Room temperature

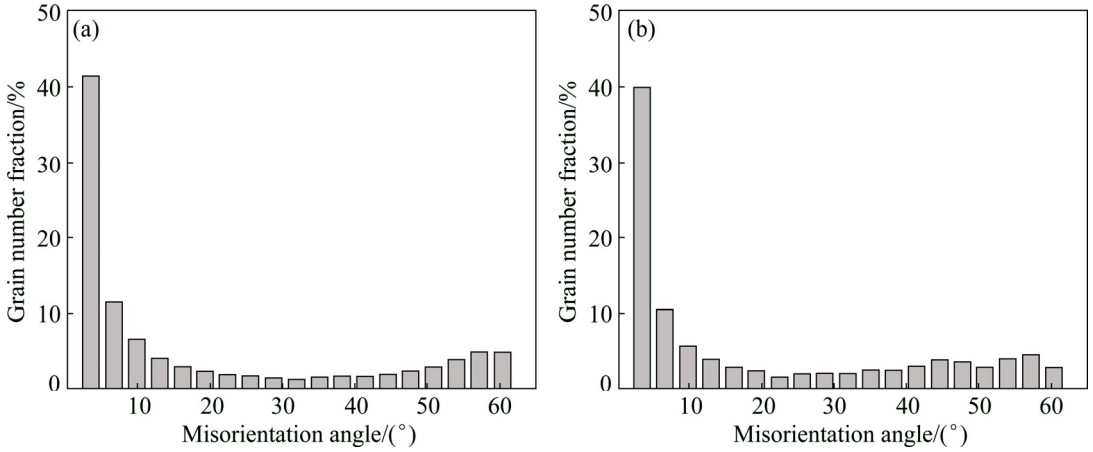

Fig. 4 Misorientation distributions of Cu−0.23%Al_2O_3 alloy forged at different temperatures: (a) Cryogenic temperature; (b) Room temperature

Cryogenic deformation conducted important effect on refining grain size of the alloy.

3.2 Deformation texture

The results of X-ray texture analysis are shown in Fig. 6. The density peaks in ODF maps indicated that Brass and Cube textures formed during hot extrusion process (Fig. 6(a)). Brass, Goss and S textures were observed after forging deformation at CT with a reduction of 80% (Fig. 6(b)), while only Brass and Goss textures were observed in specimens forged at RT (Fig. 6(c)).

Figure 7 shows the texture evolution of Cu−0.23%Al_2O_3 alloy, on the basis of calculation results. Fractions of Brass, Goss and S components in the alloy markedly increased after cryogenic forging. Compared with the hot-extruded alloy, fractions of Brass, Goss and S components in alloy forged at CT increased from 20% to 29%, 1% to 27% and 0 to 14%, respectively. While in alloy forged at RT, Brass increased from 20% to 28% and Goss increased from 1% to 20%.

3.3 Analysis of texture evolution

Texture types of the deformed pure copper and copper alloy were mainly affected by the stacking fault energy (SFE) and deformation mechanism [15,16]. Since dispersed Al_2O_3 nano-particles had little effect on Cu atoms arrangement, SFE of Cu−0.23%Al_2O_3 alloy and that of pure copper were considered to be equal [17,18]. The main texture type in the pure copper deformed at RT was Copper texture. However, it was transformed into Brass texture as pure copper was deformed at CT. It was attributed to the suppression of dislocations cross-slip for the main texture of pure copper transformation from Copper texture to Brass texture [19]. The main texture transformation in Cu−Al_2O_3 alloy from Copper texture to Brass texture can be explained by the same reason as in pure copper. The main texture type in hot-extruded Cu−Al_2O_3 alloy was Brass texture, which increased obviously in specimens deformed at CT or RT. Dislocations cross-slip was suppressed at CT. Al_2O_3 nanoparticles pinned dislocations effectively and blocked cross-slip of dislocations. Thus, Brass texture increased

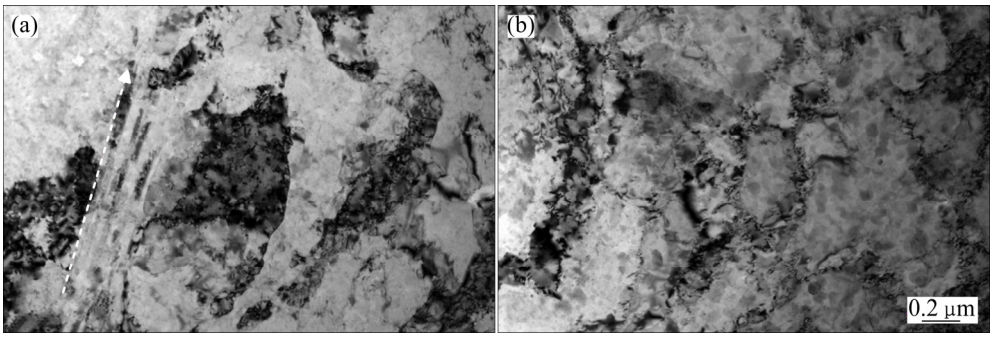

Fig. 5 TEM images of microstructure formed in Cu−0.23%Al_2O_3 alloy forged at different temperatures: (a) Cryogenic temperature; (b) Room temperature

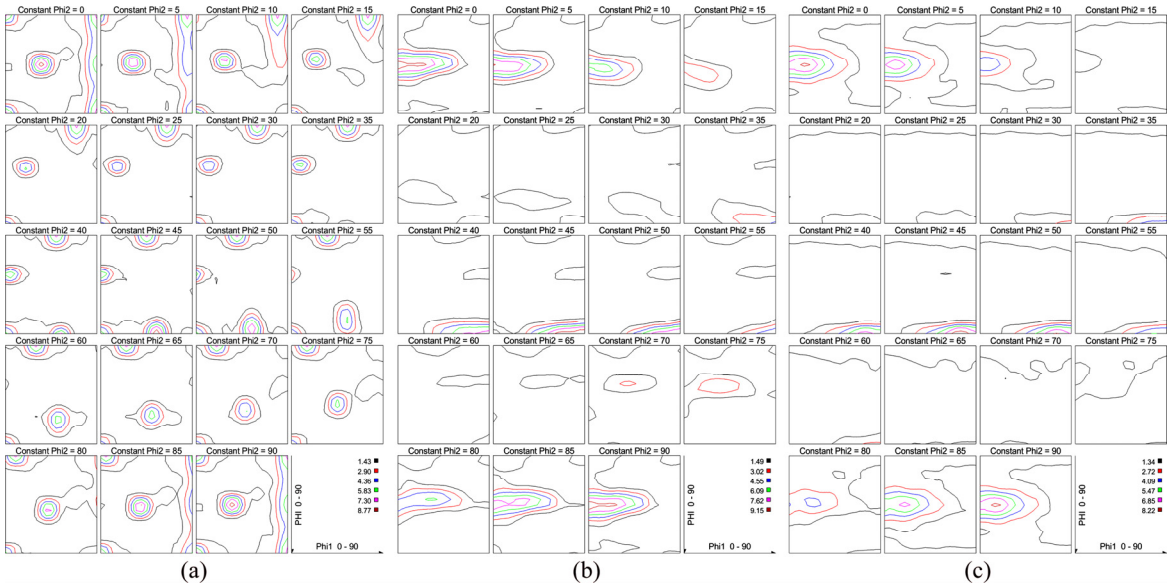

Fig. 6 ODF maps of hot-extruded Cu−0.23%Al_2O_3 alloy (a) and specimens forged at cryogenic temperature (b) and room temperature (c)

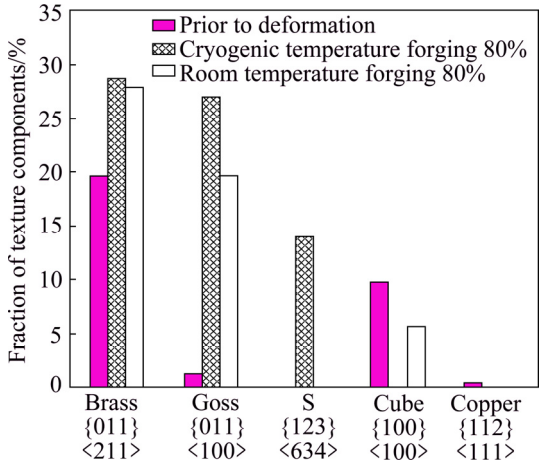

Fig. 7 Fractions of texture components in Cu−0.23%Al_2O_3 alloy with different states

in specimens forged at CT or RT.

Figure 8 shows the schematic diagram of textures transition from Copper texture to Brass texture. During the deformation process in face centered cube alloys, grains with Copper orientation firstly rotated to Goss orientation, and then those with Goss orientation rotated to Brass orientation. Here, Goss could be considered as a transition component. Grains rotated via dislocations slipping or grain boundaries migration during the texture evolution. In Cu−Al_2O_3 alloy forged at CT, dislocations slipping and migration of grain boundaries were suppressed by both cryogenic temperature and pinning effect from Al_2O_3 nanoparticles. While in Cu−Al_2O_3 alloy forged at RT, dislocations slipping and migration of grain boundaries were suppressed only by pinning effect from Al_2O_3 nanoparticles. As a result, texture evolution became harder and more transition component (Goss texture) was retained; and therefore a stronger Goss texture formed in specimens forged at CT. Besides, a strong S orientation might occur at an intermediate stage of texture evolution [20]. Texture transition in the specimens forged at CT was harder, and textures in Cu−Al_2O_3 alloy forged at CT were more likely to represent intermediate stages of texture evolution. Therefore, S texture appeared not in specimens forged at RT but in those forged at CT. This result indicated that cryogenic temperature was beneficial to the formation of S texture in Cu−Al_2O_3 alloy during deformation process.

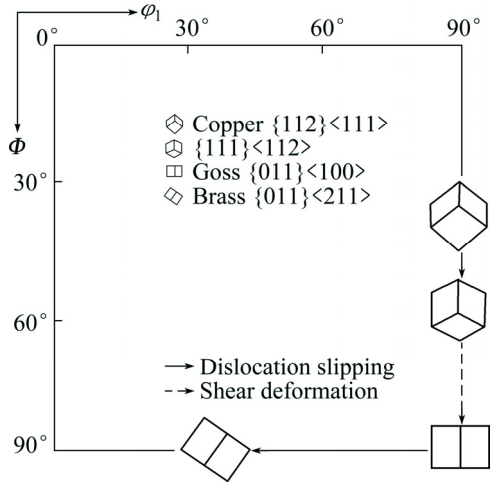

Fig. 8 Schematic diagram of texture transition from Copper to Brass of Cu−0.23%Al_2O_3 alloy (ODF φ_2=45°)

4 Conclusions

1) The main textures in hot-extruded specimen were Brass {011}⟨211⟩ and Cube {100}⟨100⟩ texture. Textures of Brass {011}⟨211⟩ and Goss {011}⟨100⟩ formed in specimen deformed at room temperature, while textures of Brass {011}⟨211⟩, Goss {011}⟨100⟩ and S {123}⟨634⟩ formed in specimen deformed at cryogenic temperature. No S component was observed in alloy deformed at room temperature.

2) Compared with the hot-extruded alloy, fractions of Brass, Goss and S components in alloy forged at CT increased from 20% to 29%, 1% to 27% and 0 to 14%, respectively. While, Brass and Goss textures in alloy forged at RT increased from 20% to 28% and 1% to 20%, respectively.

3) Al_2O_3 nanoparticles has pinning effect on dislocations, which can further lead to the suppression of dislocations cross-slip. This can well explain the formation of Brass and Goss textures in the specimen deformed at room temperature. While in the specimen deformed at cryogenic temperature, both pinning effect and cryogenic temperature are responsible for the formation of Brass, Goss and S. It is believed that cryogenic temperature was beneficial to the formation of S{123}⟨634⟩.

References

[1] MARY J A, MANIKANDAN A, KENNEDY J L, OUOUDINA M, SUNDARAM R, VIJAYA J J. Structure and magnetic properties of Cu−Ni alloy nanoparticles prepared by rapid microwave combustion method [J]. Transactions of Nonferrous Metals Society of China, 2014, 24(5): 1467−1473.

[2] SAN Xing-yuan, LIANG Xiao-guang, CHENG Lian-ping, SHEN Li, ZHU Xin-kun. Effect of stacking fault energy on mechanical properties of ultrafine-grain Cu and Cu−Al alloy processed by cold-rolling [J]. Transactions of Nonferrous Metals Society of China, 2012, 22(4): 819−824.

[3] GUO Ming-xing, WANG Ming-pu. The compression characteristics of particle-containing Cu alloys under different conditions [J]. Materials Science and Engineering A, 2012, 556: 807−815.

[4] YU Qing-chun, ZHANG Shi-chao, YANG Bin. Dispersion of copper oxide supported on γ-alumina and its sulfation properties [J]. Transactions of Nonferrous Metals Society of China, 2011, 21(12): 2644−2648.

[5] CHANDRASEKHAR S B, SUDHAKARA SARMA S, RAMAKRISHNA M, SURESH B P, RAO T N, KASHYAP B P. Microstructure and properties of hot extruded Cu−1wt% Al_2O_3 nano-composites synthesized by various techniques [J]. Materials Science and Engineering A, 2014, 591: 46−53.

[6] GUO Ming-xing, WANG Ming-ping. Effects of particle size, volume fraction, orientation and distribution on the high temperature compression and dynamical recrystallization behaviors of particle-containing alloys [J]. Materials Science and Engineering A, 2012, 546: 15−25.

[7] CHENG Jian-yi, YU Fang-xin, DU Da-ming, MA Ming-liang. Influence of nano-scaled dispersion second phase on substructure of deformation dispersion strengthened copper alloy [J]. Powder Metallurgy Industry, 2010, 20(2): 27−31.

[8] TIAN Bao-hong, LIU Ping, SONG Ke-xing, LI Yan, LIU Yong, REN Feng-zhang, SU Juan-hua. Microstructure and properties at elevated temperature of a nano-Al_2O_3 particles dispersion-strengthened copper base composite [J]. Materials Science and Engineering A, 2006, 435−436: 705−710.

[9] DAS M, PAL T K, DAS G. Effect of aging and cryo rolling on microstructural characterization and mechanical properties of precipitation hardenable 6063Al alloy [J]. Materials Science and Engineering A, 2012, 552: 31−35.

[10] LUAN Bai-feng, YE Qing, CHEN Jian-wei, YU Hong-bing, ZHOU Dong-li, XIN Yun-chang. Deformation twinning and textural evolution of pure zirconium during rolling at low temperature [J]. Transactions of Nonferrous Metals Society of China, 2013, 23(10): 2890−2895.

[11] NIRANJANI V L, HARI KUMAR K C, SUBRAMANYA SARMA V. Development of high strength Al−Mg−Si AA6061 alloy through cold rolling and ageing [J]. Materials Science and Engineering A, 2009, 515(1−2): 169−174.

[12] HUANG Y, PRANGNELL P B. The effect of cryogenic temperature and change in deformation mode on the limiting grain size in a severely deformed dilute aluminium alloy [J]. Acta Materialia, 2008, 56(7): 1619−1632.

[13] CHENG Jian-yi, WANG Ming-pu, LI Zhou, FANG Shan-feng, GUO Ming-xing, LIU Shi-feng. Cold drawing and annealing behavior of nano-sized Al_2O_3 dispersion strengthened copper [J]. Rare Metall Materials and Engineering, 2004, 33(11): 1178−1181.

[14] TANG Jian-guo, ZHANG Xin-ming, DENG Yun-lai, DU Yu-xuan, CHEN Zhi-yong. Texture decomposition with particle swarm optimization algorithm method [J]. Computational Materials Science, 2006, 38(1−2): 395−399.

[15] SIDOR J J, KESTENS L. Analytical description of rolling textures in face-centered-cubic metals [J]. Scripta Materialia, 2013, 68(5): 273−276.

[16] LEFFERS T, RAY R K. The brass-type texture and its deviation from the copper-type texture [J]. Progress in Materials Science, 2009, 54(3): 351−396.

[17] YAKUBTSOV I A, ARIAPOUR A, PEROVIC D D. Effect of nitrogen on stacking fault energy of F.C.C. iron-based alloys [J]. Acta Materialia, 1999, 47(4): 1271−1279.

[18] SMIRNOV A A. The molecular kinetic theory of metals [M]. Moscow: Nauka, 1966.

[19] JIANG Shu-yong, ZHANG Yan-qiu. Microstructure evolution and deformation behavior of as-cast NiTi shape memory alloy under compression [J]. Transactions of Nonferrous Metals Society of China, 2012, 22(1): 90−96.

[20] HIRSCH J, LUCKE K. Overview No. 76: Mechanism of deformation and development of rolling textures in polycrystalline F.C.C. metals—I. Description of rolling texture development in homogeneous Cu−Zn alloys [J]. Acta Metallurgica, 1988, 36(11): 2863−2882.

$Cu-A1_2O_3$ 弥散强化铜合金在不同条件下变形的显微组织与结构演变

李 灵[1]，李 周[1,2]，雷 前[2]，肖 柱[3]，刘 斌[1]，刘 娜[1]

1. 中南大学 材料科学与工程学院，长沙 410083；
2. 中南大学 粉末冶金国家重点实验室，长沙 410083；
3. 中南大学 有色金属材料与工程教育部重点实验室，长沙 410083

摘 要：对 $Cu-0.23\%A1_2O_3$ 弥散强化铜合金在超低温变形和室温变形过程中的显微组织与织构演变进行研究。结果表明：$Cu-A1_2O_3$ 弥散强化铜合金在热挤压后形成黄铜织构 Brass{011}⟨211⟩和立方织构 Cube {100}⟨100⟩；合金在室温变形后主要形成 Brass{011}⟨211⟩织构和 Goss{011}⟨100⟩织构；合金在超低温变形后主要形成黄铜织构 Brass {011}⟨211⟩、高斯织构 Goss {011}⟨100⟩和剪切织构 S {123}⟨634⟩。在室温变形过程中，决定织构类型的主要因素则仅是 Al_2O_3 纳米粒子钉扎效应产生的对位错交滑移的抑制作用。而 $Cu-A1_2O_3$ 弥散强化铜合金在超低温变形过程中，决定织构类型的主要因素包括超低温和 Al_2O_3 纳米粒子钉扎效应二者共同产生的对位错交滑移的抑制作用。

关键词：超低温变形；显微组织；织构；弥散强化铜合金

(Edited by Yun-bin HE)